EXPERIMENTAL STUDIES ON SECONDARY ELECTRON EMISSION CHARACTERISTICS OF ACCELERATOR CHAMBER MATERIALS*

S. Liu, Y. Liu†, W. Liu, G. Pei, Institute of High Energy Physics (IHEP),Chinese Academy of Sciences (CAS), [100049] Beijing, China
P. Wang†, L. Zeng, X. Sun, at Dongguan Institute of Neutron Science (DINS), [523803] Dongguan, China

Abstract

The electron multipacting effect that occurs in the accelerator vacuum tubes and radio frequency cavity has a significant impact on beam quality and normal operation of the accelerator. The multipacting effect and electron cloud effect are closely related to secondary electron emission (SEE) characteristics. In this paper, secondary electron yield (SEY), its dependence on incidence angle, spatial and energy distribution of secondary emission electrons and SEY depression as a function of deposited electron dose for Cu are measured. And the SEY of ceramic samples are successfully measured by effective charge neutralization.

INTRODUCTION

During the operation of an accelerator, the electron cloud effect in the vacuum pipe can cause beam instability and emittance growth [1-3]. The secondary electron multipacting effect occurring in the radio-frequency cavity will promote serious ignition in RF cavity, which severely limits the electromagnetic field intensity and even causes the break-up of the RF system [4]. The power deposition from secondary electron multipacting in beam screen may even lead to a quench of the entire superconductor system [5, 6]. Over the past decades, many international accelerator laboratories, such as KEK, FERMILAB, and CERN have set up an experimental apparatus to measure SEY for different materials [7-9].

In order to improve the stability on high current beam , it is necessary to select suitable material with a lower SEY to reduce the secondary electron emission. SEY can be defined as the ratio of the number of secondary electron current I_s to the number of primary electron current I_p. To study the electron cloud effect in the accelerator, a complete measurement and theoretical analysis of the SEE characteristic parameters of the accelerator vacuum chamber materials are required. The complete SEE parameters include SEY and its dependence on the incidence angle of the primary electrons, and the spatial and spectrum distribution of secondary electrons, However, there are many studies focusing on SEY and not on the other SEE parametershave been set u. So a high efficiency SEE characteristics experimental platform based on a new detector and sample holder design has been set up to measure the complete characteristic parameters of various accelerator chamber materials.

The ceramic vacuum pipe in Rapid Cycling Synchrotron of China Spallation Neutron Source (RCS/CSNS) is chosen to suppress eddy current effect produced by the rapidly changing magnetic field in dipole and quadrupole magnets of the RCS ring, but the SEY of the ceramic is so high that a TiN film is plated onto the inner wall of the ceramic vacuum pipe for suppression of SEY [10]. During the measurements on SEY for ceramics, single pulse method [11] is used to solve charge accumulation on the surface of the insulating material. The measurement results were compared with the existing experimental references which verified the reliability and practicality of the measurement method and the platform. The measurement and theoretical results of the secondary electron emission characteristics for various materials can provide a reference for selecting vacuum chamber materials with lower SEY. The measurement results can be used to improve TiN coating process and simulations of the electron cloud.

MEASUREMENT PRINCIPLE AND APPARATUS

Our measurement of the SEE characteristics is explained in Figs. 1-3. A photograph and partial view ground electrodes of the apparatus are shown in Fig. 4. As shown in Fig. 1(a), the sample holder can move up and down and even rotate from 0º to 90º within a retarding field analyser (RFA) [12]. The RFA is composed of a cap detector (connected with terminal A) and a cylindrical wall detector (connected with terminal B) with meshed grid (connected with terminal C) and meshed grid ground electrodes (connected with terminal E) inside. As shown in Fig. 3(a), there is an insulating ring between the cap detector and the wall detector for spatial distribution measurement. In order to obtain the SEY more accurately, the sample (connected with terminal D) is connected with a DC bias source. During the measurement of spectrum, the grid electrode is also connected with a DC bias source. The grounded electrode is used to shield the electrostatic field and to avoid its impact on the electron motion. SEY and its dependence on incidence angle

Because of different conductivity, there are different measuring methods for metallic conductive materials and dielectric samples as below.

High conductivity sample As shown in Fig. 1, there are two ways to measure the SEY of highly conductive metallic: sample method and collector method [13-15]. For the sample method in Fig. 1(a), when -20 V bias is set on

* Work supported by Foundation of Key Laboratory of Particle Acceleration Physics and Technology, IHEP, CAS (JSQ2016ZZ02); National Natural Science Foundation of China (U1832132, 11375215);
† email address:liuyd@ihep.ac.cn;wangpc@ihep.ac.cn

the sample, the SEs are allowed to escape from the sample surface fully and the sample current I_s is measured by picoammeter. By regulating the bias voltage to +100 V which is high enough to prevent SEs from escaping from the sample surface, the primary electron current I_p is obtained. Then the SEY is calculated by the formula δ=1-I_s/I_p. With correction on the energy of primary beam (E_p) from bias voltage 20 V, the energy calibration is included in the final results. For the collector method in Fig. 1(b), when 50 V bias is added on the detector (close K_A, and K_B connected to the ground), then the SEs are fully collected by the detector and the SE current I_s is measured. When connect the detector and the sample together with DC voltage source (Close K_A and K_B), the primary electron current I_p is obtained. Then the SEY is calculated by the formula δ=I_s/I_p. As shown in Fig. 1(a), the sample holder can be rotated axially from 0 to 180 degrees for the sake of SEY dependence on the incident angle.

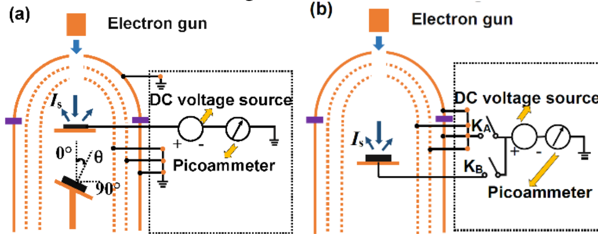

Figure 1: The schematic diagram of SEY measurement for conductive sample (a: sample method; b: collector method)

Dielectric sample Due to the poor electrical conductivity, the charge can be accumulated on the surface of dielectric sample. Therefore the key to measure the SEY of dielectric sample accurately is to eliminate the surface charge accumulation. The method based on negatively biased collector is used to neutralize the secondary electrons accumulation on the surface [11]. A pulse generator can trigger the electron gun to produce a single pulse beam with duration time 150 μs or a periodic pulse beam with repetition frequency 25 Hz, respectively for SEY measurement and charge neutralization. The schematic diagram of measurement is shown in Fig. 2. The measurement procedure is quite complex comparing to the conductive sample: firstly rotate Faraday cage up and set +45 V bias on the Faraday cup, tuning the electron gun to single pulse mode for measurement and obtain incident current I_p; secondly, rotate sample up and set +45 V bias on detector, tuning the electron gun to single pulse mode for measurement and get the secondary electron current I_s. It should be noted that before the next measurement, full neutralization procedure is required: input -45V bias on collector and then switch the electron gun to the periodic pulse mode with the pulse duration 1~ 5s to make the secondary electron return to the sample surface fully.

Spatial distribution of secondary emission electrons

For the measurement on electrons spatial distribution, the picoammeter was connected with terminal B. The experimental principle is to move the sample holder to different vertical positions and measure current variations on the cylindrical wall detector, as shown in Fig. 3(a). Assuming that the sample's initial vertical position is M and the half flare angle of the sample, the measured current on the cylindrical wall detector is I_α; after slightly moving the sample to another position N, the measured current on the wall collector is $I_{\alpha+\Delta\alpha}$ and the angle and current variation are $\Delta\alpha$ and ΔI_α= I_α- $I_{\alpha+\Delta\alpha}$, respectively. Varying the sample position step by step, the secondary electron azimuthal distribution is achieved. Using the cylindrical wall detector for obtaining the secondary electron (SE) current ΔI_α can avoid the measured electrons leakage from the aperture on the top of the cap detector.

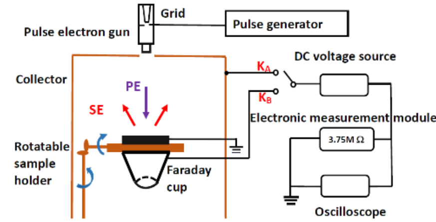

Figure 2: The schematic diagram of measurement for dielectric sample

Energy Spectrum of secondary emission electrons

The RFA which is the capped cylindrical wall detector with two meshed grid layers inside is used for scanning the secondary electron energy spectrum. By scanning the voltage on the grid layer with a DC voltage source, the energy spectrum can be obtained, as shown in Fig. 3(b). Because of the aperture on the top of the cap detector, there is some missing SE current, but these missed secondary electrons only have effect on the measured current amplitude. The secondary electrons' energy distribution will not be altered. During the measurement, the sample holder is placed at the center of the hemispherical detector. By changing the grid voltage U, the secondary electrons with energy less than eU are prevented. Then E(eU)-ΔI_s curve as energy spectrum distribution can be obtained.

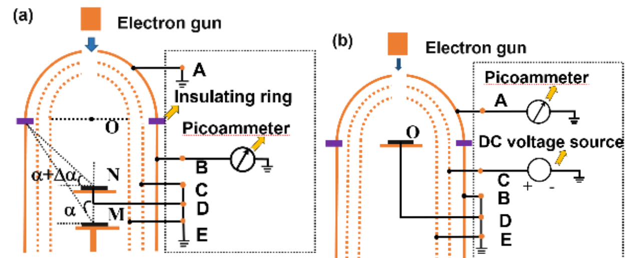

Figure 3: The schematic diagram of spatial and energy distribution measurement

SEY depression with beam deposition

The bombardment from primary beam can clean some contaminants and oxide on the surface of the sample which can cause material surface changes. Longer bombardment by primary electrons with proper energy, the surface graphitization may be produced and the presence of the carbon film can lower the measured SEY [16].

Experimental apparatus

The SEE experimental platform is composed of a vacuum system, electron gun, removable sample holder, and RFA for measuring secondary electrons. The vacuum system can keep the sample in a high vacuum environment with pressure about 10^6 Pa. The Kimball Physics EGL-7 electron gun was installed and directed toward the sample vertically, and the electron beam energy ranges from 100 eV to 5 keV with the emission current span from 1 nA to 100 μA. The maximum movable vertical distance of the sample holder is about 150 mm which corresponds to the spatial angle 10°–80°. The sample with an area of 2× 2 cm^2 and thickness of 1.5 mm can be fixed on the sample holder. The grid and ground electrodes in RFA are made of stainless steel wire cage with mesh size about 1 ×1 mm^2. An photograph and partial view of the apparatus are shown in Fig. 4.

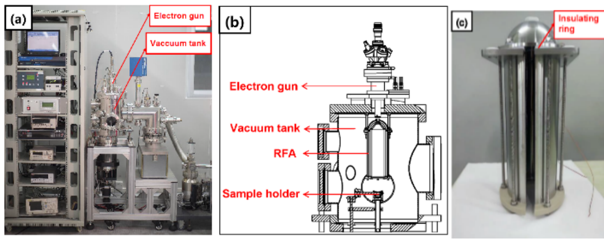

Figure 4: The partial view and photograph of the apparatus and RFA: ((a) schematic of the experimental setup, (b) partial view of experimental setup, (c) structure of RFA.)

MEASUREMENT RESULT AND THEORETICAL ANALYSIS

SEY and its dependence on incidence angle

As described before, there are two ways to measure SEY on conductive sample, such as Cu. As can be seen from Fig. 5 and Table 1, the SEYs of Cu by two methods at normal incidence are similar. Comparing the experimental results with Ref. 17, the similarity is that the primary energy E_{pm} corresponding to the maximum secondary electron are all around 300 eV. However the SEY measured by the sample method was 1.8, slightly lower than the result of Ref. 17.

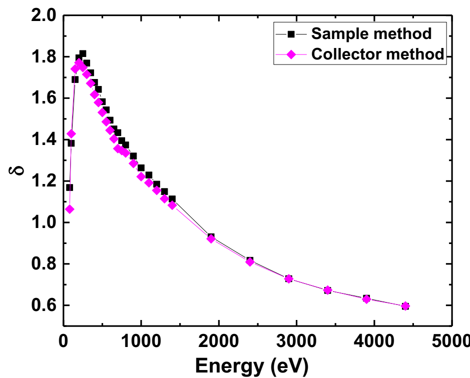

Figure 5: Primary energy and SEY of Cu measured by sample method and collector method.

Table 1: SEY of Cu measured by sample method and collector method

Cu	E_{pm} (eV)	δ_m
sample method	300	1.80
collector method	300	1.70
Valizadeh, Reza, et al.2014	300	1.90

Including conductive samples, the SEY of ceramics was measured by single pulse method in the paper. With confirmation on the SEY supression for ceramics with TiN coating, SEY of ceramics was depressed from 5.97 to 1.66 after coated with TiN and the corresponding energy E_{pm} turned from 775 eV to 230 eV as shown in Fig. 6. Therefore the SEY of untreated ceramic is high and the secondary electron yield can be effectively reduced by the TiN film plated on its inner wall.

However experimental results proved the SEY increasement (SEY~2.15) of ceramic sample with TiN after its exposure in air for 3 months as shown in Fig. 6(b). The results of SLAC show that δ_m of TiN deposited on Al and SS substrate with different impurity types were 1.5–2.4 [18]. The study in SNS indicated that δ_m of TiN plated under high and low vacuum were 1.5–1.6 and 2.0–2.7 [19], respectively; At J-PARC, δ_m was about about 1.6 [20]. According to reference [21], δ_m of ceramic was about 6.4. Therefore, the measured results in the CSNS shown in Table. 1 basically agree with the value of the references.

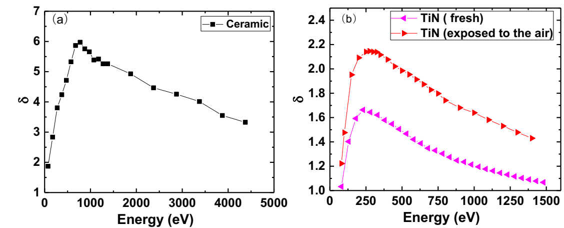

Figure 6: SEY of ceramic sample before and after coated with TiN.

The secondary electron yield under oblique incidence can be measured by rotating the sample holder. As shown in Fig. 7, the SEY gradually increases with the increase of the incident angle θ in the range of 0-60°, with a cosine relationship on incident angle θ, which is consistent with the reference [22]. However, the SEY begins to decrease after the incident angle increased to 60°, which is because the measurement error increases with the increase of the incident angle θ. The result above 60° is not shown in Fig. 7 because of measurement error .

$$y = \cos(\theta)^{-n} \tag{1}$$

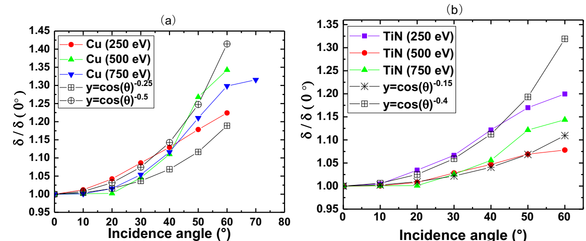

Figure 7: SEY at different incident angle

Table 2: E_{pm} and δ_m of ceramic with and without TiN

Sample	E_{pm}(eV)	δ_m	E_p (reference)	δ_m (reference)
ceramic	775	5.97	650	6.4
coated with TiN (fresh)	230	1.66	300	1.5~2.4

In Eq. 1, n is the coefficient related to the energy of the material and the incident beam, y is a cosine function of θ and n. Comparing the measurement results with calculation results of the cosine function formula, it can be seen that the corresponding coefficients n of several materials ranges from about 0.16 to 0.80.The corresponding values of n for different materials are shown in Table 2.

Spatial distribution of secondary emission electrons

According to the theory [23], the number of true secondary electrons per polar angle is described by following formula:

$$f(\theta) = \cos\theta(1 + a\sin^2\theta + b\sin^4\theta + ...) \quad (2)$$

where a, b, and c are the coefficients decided by the smallest momentum which electrons need to escape the sample. According to Eq. 2, the parameters obtained by fitting the measurement results of Cu and TiN using Eq. 2 are shown in Figure 8 and Table. 3. Therefore the secondary electrons' spatial distribution measured in the experiment is consistent with the theoretical results and Ref. 24. The difference is that the elastic scattering electrons are unconcerned in the theoretical formula, while all kinds of the secondary electrons are included in the experimental data.

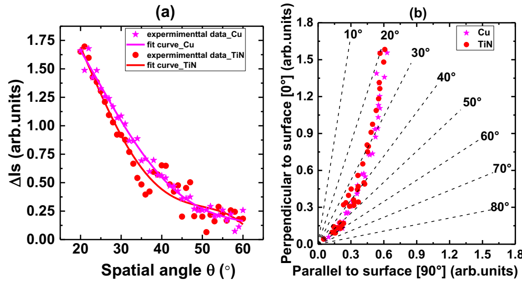

Figure 8: SE spatial distribution in cartesian and polar coordinate systems

Table 3: Fitting parameters spatial distribution

	a	b
Cu	-2.10	1.63
TiN(ceramic substrate)	-1.24	1.91

Energy Spectrum of secondary emission electrons

The SE energy spectrum is measured by RFA [25] and the results are shown in Fig. 9-11. According to the normal secondary electron emission model [26], the SEs are composed of three portions: "true" secondary electron (SE) with the lower energy range 0-50 eV; elastic reflected secondary electron (ERSE) which are emitted with almost the same energy as the incident particles; and inelastic reflected secondary electron (IRSE) or "rediffused" electrons with a uniform energy spectrum from 50 eV to the incident particle energy. For this experiment on the Cu sample, the "true" secondary electron energy ranged from 0 to 50 eV with peak at about 1.5-2.5 eV which does not change with the energy of incident electrons. Because of the aperture on the top of the cap detector for the primary beam passing through, which corresponds to a vertical azimuth about 25°, much of the "elastic" electrons can escape from the aperture which leads to the lower measured current of "elastic" electrons in Fig. 10. Comparing the measured energy spectrum with Ref. 27, it is clear that the "elastic" electrons whose energy is the same with that of primary electrons are also confirmed in our experiments. But due to strict experimental requirements in Ref. 27 such as lower energy primary electrons (3.17 eV–312 eV), accurate energy analyzer, and cryogenic environment (9 K), the portion of reflected electrons and its dependency on low primary energy are less accurately measured in our experiments.

As shown in Table. 4, we can conclude that the percentage for true SE is more than 80% of the total emission electrons. The position of the true secondary electron peak changes very little with the change of the energy of the incident electron as shown in Fig. 11, but the position of the elastic scattering peak increases with the increase of the energy of the incident electron as shown in Fig. 10. This is because of different generation mechanism. The true SE come from extranuclear electrons and the elastic electron come from primary electrons [26].

The width at half maximum (FWHM) [12] of the true secondary electron peak and the elastic reflected electron peak are fitted in Table. 5 and marked in the Fig. 10. In the Ref. [28], FWHM for the secondary electron spectra of polycrystalline Cu is 5.1 eV and the position of the peak is 1.3 eV when the incidence energy is 1.5 keV which is consisitent with the measurement results.

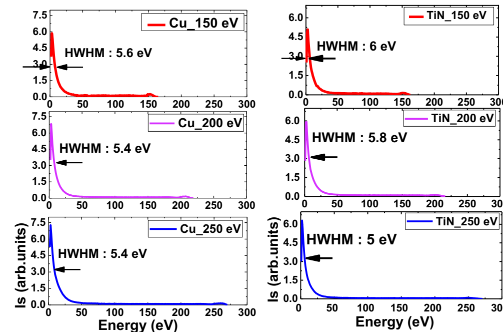

Figure 9: Total secondary electron energy spectrum of Cu and TiN on ceramic.

Table 4: The proportion of secondary electrons composition.

Sample	E_p(eV)	SE	ERSE	IRSE
Cu	150	80.2%	4.8%	15.0%
	200	79.9%	3.1%	17.0%
	250	76.8%	2.9%	20.3%
TiN	150	81.8%	3.3%	14.9%
	200	78.7%	3.5%	17.8%
	250	78.5%	3.0%	18.5%

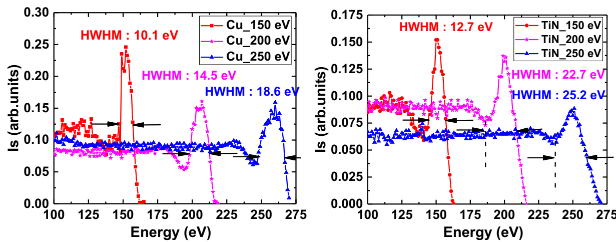

Figure 10: ERSE energy spectrum of Cu and TiN on ceramic.

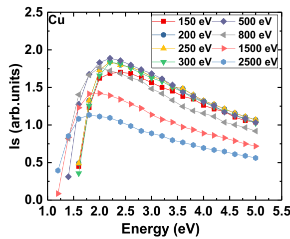

Figure 11: SE energy spectrum of Cu

Table 5: FWHM of the true secondary electron peak and the elastic reflected electron peak

Sample	E_p (eV)	SE (eV)	ERSE (eV)
Cu	150	5.6	10.1
	200	5.4	14.5
	250	5.4	18.6
TiN	150	6.0	12.7
	200	5.8	22.7
	250	5.0	25.2

SEY depression as electron dose deposition

According to Refs. 16 and 29-31, incident electron bombardment can cause surface changes of the material, such as clearance of some contaminants and oxide. In order to understand the "dose" effect, the SEY is measured for different depositions of primary beam. Fixing the primary beam energy and current with continuous bombardment on the sample for 10 hours, the maximum SEY decreases with the increase of incident electron dose and finally stabilizes as shown in Fig. 12. As shown in Table. 6, the charge deposition of 3.13×10^{-3} C/mm², the maximum SEY of Cu and TiN drops from 1.81 to 1.46 .Therefore bombardment reducing SEY is an effective secondary electron suppression measure [16].

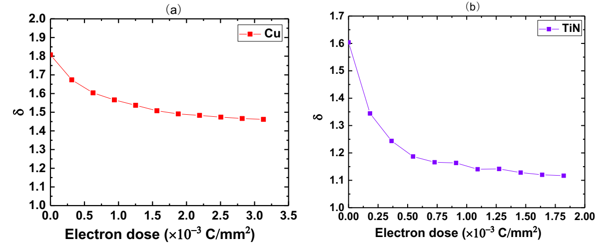

Figure 12: SEY as a function of electron dose

Table. 6: SEY before and after electron bombardment

Sample	δ_0	δ	Dose ($\times10^{-3}$C/mm^2)
Cu	1.81	1.46	3.13
TiN	1.60	1.12	1.82

CONCLUSION

In order to study the SEE characteristics of accelerator vacuum chamber materials, a novel experimental apparatus for SEE measurements was set up in CSNS. SEY, spatial distribution, energy spectrum, and "dose" effect were obtained by this device. SEY on conductive samples measured by sample method and collector method at normal incidence are coincident. Due to the poor electrical conductivity, single pulse method is used for measurement on SEY of dielectric sample to reduce charge accumulation phenomenon on the surfaces. The negative bias collector method can be used to neutralize the secondary electrons accumulation on the surface of insulating sample effectively. The measurement results proved the SEY dependence on incidence angle and spatial angle SE spatial distribution can be parametrized with a cosine relation. The "true" secondary electron energy range (<50 eV) for different materials have been verified in energy distribution measurements. The experimental results demonstrated the availability of measurement methds and validated the the apparatis structure.

REFERENCES

[1] K. Ohmi, F. Zimmermann, "Head-Tail Instability Caused by Electron Clouds in Positron Storage Rings," Phys. Rev. Lett. 85, 3821 (2000).

[2] M. Tobiyama, J. W. Flanagan, H. Fukuma, S. Kurokawa, K. Ohmi, and S. S. Win, "Coupled bunch instability caused by an electron cloud," Phys. Rev. ST Accel. Beams 9, 012801 (2006).

[3] C. M. Lyneis, H. A. Schwettman, J. P..Turneaure, "Elimination on electron multipacting in superconducting structures for electron accelerators". Applied Physics Letters, 1977, 31(8): 541-543.

[4] R. Prakash, A. R. Jana, V. Kumar. "Multipacting studies in elliptic SRF cavities". Nuclear Instruments and Methods in Physics Research Section A: Accelerators, Spectrometers, Detectors and Associated Equipment, 2017, 867: 128-138.

[5] R. Cimino and T. Demma, "Electron cloud in accelerators", Int. Journal of Modern Phys. A, vol. 29, no. 17, p. 1430023, 2014.

[6] R. Cimino, V. Baglin and F. Schäfers. Potential remedies for the high synchrotron-radiation-induced heat load for future highest-energy-proton circular colliders. Physical review letters, 2015, 115(26): 264804.

[7] R. Cimino et al., "Detailed investigation of the low energy secondary electron yield of technical Cu and its relevance for the LHC", Physical Review Special Topics-Accelerators and Beams, vol. 18, no. 5, p. 051002, 2015

[8] K. Yamamoto et al., "Secondary electron emission yields from the J-PARC RCS vacuum components", Vacuum, vol.81, no. 6, pp 788-792, 2007.

[9] Y. Ji, L. Spentzouris and R. Zwaska, "Update of the SEY Measurement at Fermilab Main Injector", in Proc. NAPAC' 16, Chicago, IL, USA, Oct. 2016.doi:10.18429/JACOW-NAPAC2016-THPOA45

[10] H. Dong, H. Song, Q. Li et al., The vacuum system of the China spallation neutron source. Vacuum, 2018, 154: 75-81.

[11] M. Weng, M. Cao, H. J. Zhao et al. Note: A simple charge neutralization method for measuring the secondary electron yield of insulators. Review of Scientific Instruments, 2014, 85(3): 036108.

[12] P. Staib, U. Dinklage. "Recent developments on an improved retarding-field analyser". Journal of Physics E: Scientific Instruments, 1977, 10(9): 914.

[13] Ji. Yichen, Linda Spentzouris and Robert Zwaska. "Secondary electron yield measurement and electron cloud simulation at Fermilab". (2015): MOPMA039.

[14] K. Yamamoto, T. Shibata, N. Ogiwara et al., "Secondary electron emission yields from the J-PARC RCS vacuum components". Vacuum, 2007, 81(6): 788-792.

[15] H. Miyake, K. Nitta, Michizono S, et al. "Secondary electron emission on degradation sample and development of new measurement system with low electron energy". Discharges and Electrical Insulation in Vacuum, 2008. ISDEIV 2008. 23rd International Symposium on. IEEE, 2008, 2: 553-556.

[16] R. Cimino et al., "Electron energy dependence of scrubbing efficiency to mitigate e-cloud formation in accelerators", in Proc. EPAC08, Genoa, Italy, 23-27 June 2008, paper TUPP027, pp.1592–1594.

[17] R. Valizadeh, O. B. Malyshev, S. Wang et al., "Low secondary electron yield engineered surface for electron cloud mitigation". Applied Physics Letters, 2014, 105(23): 231605.

[18] F. L. Pimpec, R.E. Kirby, F. King et al., Properties of TiN and TiZrV thin film as a remedy against electron cloud, Nucl. Instrum. Meth. Phys. Res. Sect. A 551 (2–3) (2005) 187–199.

[19] P. He, B. Henrist, F. L. Pimpec et al., "Secondary electron emission measurements for TiN coating on the stainless steel of SNS accumulator ring vacuum chamber". No. EPAC-2004-WEPKF085. 2004.

[20] K. Yamamoto, T. Shibata, N. Ogiwara et al. "Secondary electron emission yields from the J-PARC RCS vacuum components". Vacuum, 2007, 81(6): 788-792.

[21] P. Dawson, "Secondary electron emission yields of some ceramics", J. Appl. Phys. 37(9) (1966) 3644–3645.

[22] M. Commisso, P. Barone, A. Bonanno et al. "Angular dependence of secondary electron emission from Cu surfaces induced by electron bombardment". Journal of Physics: Conference Series. IOP Publishing, 2008, 100(9): 092013

[23] E. M. Baroody. "A theory of secondary electron emission from metals". Physical Review, 1950, 78(6): 780.

[24] J. L. H. Jonker, "The angular distribution of the secondary electrons of nickel". Philips Research Reports, 1951, 6(5): 372-387.

[25] T. Koshikawa, R. Shimizu. "Secondary electron and backscattering measurements for polycrystalline copper with a spherical retarding-field analyser". Journal of Physics D: Applied Physics, 1973, 6(11): 1369.

[26] H. Seiler. "Secondary electron emission in the scanning electron microscope". Journal of Applied Physics, 1983, 54(11): R1-R18.

[27] R. Cimino, I. R. Collins. "Vacuum chamber surface electronic properties influencing electron cloud phenomena". Applied surface science, 2004, 235(1-2): 231-235.

[28] T. Koshikawa, R. Shimizu. "Secondary electron and backscattering measurements for polycrystalline copper with a spherical retarding-field analyser". Journal of Physics D: Applied Physics, 1973, 6(11): 1369.

[29] R. Larciprete, D. R. Grosso, M. Commisso et al. "The chemical origin of SEY at technical surfaces". arXiv preprint arXiv:1308.1290, 2013.

[30] V. Baglin, "The Secondary Electron Yield of Technical Materials and its Variation with Surface Treatments," LHC-Project-Report-433, Proc. 7th European Particle Accelerator Conference, Vienna, Austria, 26 - 30 Jun 2000, pp. e-proc. 217 (2000).

[31] V. Baglin, I. Collins, B. Henrist, N. Hilleret, G. Vorlaufer, "A Summary of Main Experimental Results Concerning the Secondary Electron Emission of Copper," LHC-Project-Report-472 ; CERN-LHC-Project-Report-472 (2001).